

# JGR Atmospheres

## RESEARCH ARTICLE

10.1029/2021JD035355

### Key Points:

- Estimates of shallow convective mixing in shallow cumulus regions are developed using satellite retrievals of water vapor isotopes
- Strong shallow convective mixing is associated with moistening of the free troposphere in the tropics
- The relationship between shallow convective mixing and low-cloud fraction is spatially variable in shallow cumulus regions

### Supporting Information:

Supporting Information may be found in the online version of this article.

### Correspondence to:

J. Hu,  
[hujun@xmu.edu.cn](mailto:hujun@xmu.edu.cn)

### Citation:

Hu, J., Bailey, A., Nusbaumer, J., Dee, S., Sasser, C., & Worden, J. (2022). Tracking shallow convective mixing and its influence on low-level clouds with stable water isotopes in vapor. *Journal of Geophysical Research: Atmospheres*, 127, e2021JD035355. <https://doi.org/10.1029/2021JD035355>







Received 2 JUN 2021

Accepted 11 FEB 2022

### Author Contributions:

**Conceptualization:** Adriana Bailey  
**Formal analysis:** Jun Hu, Christiana Sasser  
**Funding acquisition:** Adriana Bailey, Jesse Nusbaumer, Sylvia Dee  
**Investigation:** Jun Hu, Adriana Bailey  
**Project Administration:** Adriana Bailey, Jesse Nusbaumer, Sylvia Dee  
**Resources:** John Worden  
**Supervision:** Adriana Bailey, Jesse Nusbaumer, Sylvia Dee  
**Visualization:** Jun Hu, Christiana Sasser  
**Writing – original draft:** Jun Hu  
**Writing – review & editing:** Jun Hu, Adriana Bailey, Jesse Nusbaumer, Sylvia Dee, John Worden

## Tracking Shallow Convective Mixing and Its Influence on Low-Level Clouds With Stable Water Isotopes in Vapor

Jun Hu<sup>1,2</sup> , Adriana Bailey<sup>3</sup> , Jesse Nusbaumer<sup>3</sup> , Sylvia Dee<sup>1</sup> , Christiana Sasser<sup>4,5</sup> , and John Worden<sup>6</sup> 

<sup>1</sup>Department of Earth, Environmental and Planetary Science, Rice University, Houston, TX, USA, <sup>2</sup>College of Ocean and Earth Sciences, Xiamen University, Xiamen, China, <sup>3</sup>National Center for Atmospheric Research, Boulder, CO, USA, <sup>4</sup>Cooperative Science Center for Earth Systems Sciences and Remote Sensing Technologies, National Oceanic and Atmospheric Administration, Baltimore, MD, USA, <sup>5</sup>Department of Mechanical Engineering, University of Maryland, Baltimore, MD, USA, <sup>6</sup>Jet Propulsion Laboratory, California Institute of Technology, Pasadena, CA, USA

**Abstract** Low-cloud feedbacks contribute large uncertainties to climate projections and estimated climate sensitivity. A key physical process modulating low-cloud feedbacks is shallow convective mixing between the boundary layer and the free troposphere. However, there are challenges in acquiring observational constraints of shallow convective mixing with global coverage. To this end, we propose a novel approach to constraining convective mixing using stable water vapor isotope profiles from satellite retrievals. We demonstrate that the vertical gradient of water vapor  $\delta D$  between the boundary layer and free troposphere can be used to track shallow convective mixing. Analyzing isotopes in water vapor alongside low-cloud properties from satellite retrievals, we find that low-cloud fraction appears largely insensitive to convective mixing in shallow cumulus regions. Our results also suggest that strong shallow convective mixing is associated with the moistening of the free troposphere. The new estimate of shallow convective mixing and its relationship with low-cloud properties offers a potential constraint on simulations of low-cloud feedbacks and estimates of climate sensitivity.

## 1. Introduction

Cloud processes in climate models contribute large uncertainties to predictions of future climate (Boucher et al., 2013). In particular, low-cloud feedbacks have been shown to contribute to the simulated increase in equilibrium climate sensitivity in the latest generation of coupled general circulation models (GCMs; Zelinka et al., 2020). A key physical process modulating low clouds is shallow convective mixing between the boundary layer and the free troposphere, which may explain up to half of the variance in climate sensitivity estimates from a collection of CMIP3 and CMIP5 models (Sherwood et al., 2014). Shallow convective mixing transports moisture upward, moistening the lower troposphere and drying the boundary layer; this potentially suppresses further developments of low-level clouds, allowing shortwave radiation to pass through the atmosphere and warm the Earth's surface. This proposed mechanism could amplify global warming in the future (Blossey et al., 2013; Brient et al., 2016; Vial et al., 2016; Figure 1). However, some Large-Eddy simulations (LES) suggest that GCMs may erroneously amplify this positive feedback. Most LES suggest that cloud fraction is largely insensitive to variations in the strength of shallow convective mixing (Vial et al., 2017). Therefore, the role of shallow convective mixing in regulating the low-cloud feedback in nature is still debated.

The importance of shallow convective mixing processes in future warming projections necessitates global observations and monitoring. At present, we have spatially limited observations of shallow convective mixing (Rauber et al., 2007; Rémillard et al., 2012) from the Barbados Cloud Observatory (BCO; Nuijens et al., 2015a) and recent field campaigns including EUREC<sup>4</sup>A (Elucidating the Role of Clouds-Circulation Coupling in Climate; Stevens et al., 2021). While these and other studies have collected invaluable aircraft and ship-based *in situ* observations of mixing in the trade cumulus environment, estimates of shallow convective mixing spanning broad regions and a wide range of environmental conditions are lacking.

A number of methods can potentially be applied to estimate shallow convective mixing over large spatial scales. For example, Sherwood et al. (2014) used the difference of temperature and relative humidity between 700 and 850 hPa to estimate shallow convective mixing in climate models. However, shortwave and longwave radiation influence temperature and relative humidity, potentially obfuscating the mixing signal. In addition, it is possible to use vertical gradients of specific humidity to estimate shallow convective mixing. However, both increased

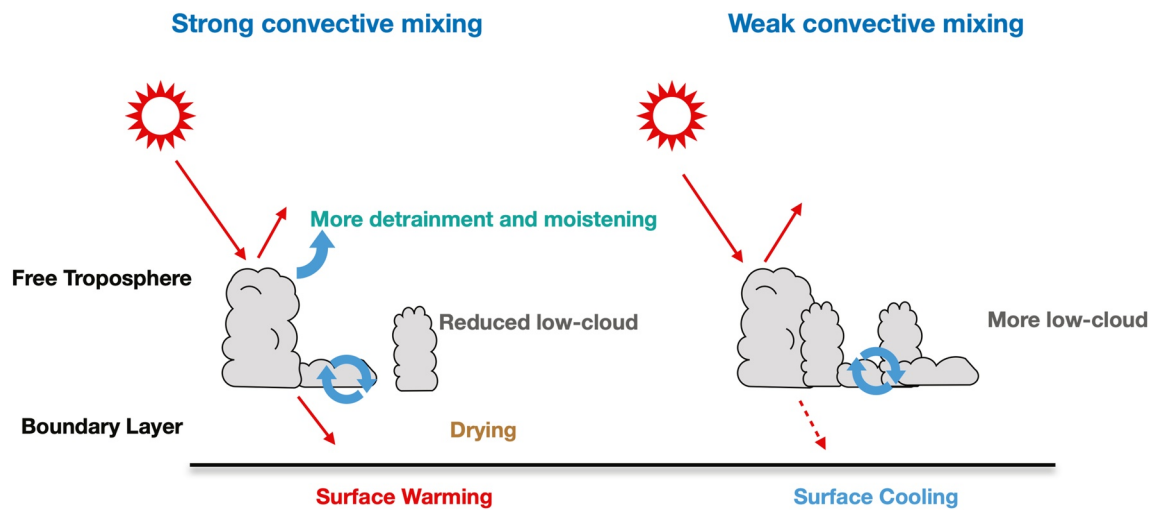


**Figure 1.** Schematic of proposed impacts of shallow convective mixing on low-level clouds simulated in climate models. Surface warming can lead to increased shallow convective mixing, which dries the boundary layer and suppresses the formation of low clouds. The reduction in low clouds allows more radiation to reach the ground, increasing surface temperature.

vertical mixing and condensation and reevaporation processes in deep convection reduce specific humidity gradients, confounding the interpretation of the specific humidity gradient.

In comparison, water vapor isotopes house the potential to provide a novel metric to estimate shallow convective mixing because they can help disentangle the impacts of shallow convective mixing versus deep convection on moistening the lower free troposphere. (While the change in isotopic composition through condensation processes does depend on temperature, the dependence is weak, and its effect is negligible on large spatial scales, Bailey et al., 2018; Siler et al., 2021). Specifically, shallow convective mixing is more effective in reducing the vertical isotopic gradient in the lower troposphere due to the fact that isotopic enrichment caused by relatively unmixed ascent in deep convective plumes is buffered by the depleting effects of condensation and precipitation processes. Moreover, the vertical gradient of water vapor  $\delta D$  between the boundary layer and the free troposphere is generally large (with a magnitude on the order of  $\sim 100\text{‰}$ ), increasing the probability of detecting variations of the vertical gradient with satellite sensors. The  $\delta D$  notation is an expression for the ratio of water vapor HDO and  $\text{H}_2\text{O}$ . It is calculated as  $\delta D = (R_D/R_{VSMOW} - 1) \times 1,000$ , where  $R_D = \text{HDO}/\text{H}_2\text{O}$ , and  $R_{VSMOW}$  is the standard HDO/ $\text{H}_2\text{O}$  ratio of Vienna Standard Mean Ocean Water. Water vapor  $\delta D$  is more positive in the boundary layer due to regular replenishment from the surface ocean, while water vapor  $\delta D$  in the free troposphere is more negative. The export of boundary layer moisture into the free troposphere via convective mixing causes free tropospheric water vapor  $\delta D$  to become less negative, reducing the vertical gradient in water isotope ratios (Bailey et al., 2013; Berkelhammer et al., 2012; Galewsky et al., 2007, 2016; Noone et al., 2011). Crucially, we have satellite retrievals of water vapor isotopes spanning more than a decade, and covering all regions between  $60^\circ\text{S}$  and  $60^\circ\text{N}$  (Worden et al., 2006, 2019).

Given the above-mentioned advantages of water vapor isotopes, this study proposes a new approach and proof-of-concept for constraining the spatiotemporal variability of shallow convective mixing using stable water isotope profiles from satellite retrievals, which provide broad spatial coverage. We demonstrate that isotope ratios of water vapor can be used to distinguish between periods of strong and weak convective mixing, due to the fact that isotope ratios are distinctly different between the marine boundary layer and the free troposphere. Therefore, the vertical difference of water vapor  $\delta D$  (or the isotopic lapse rate) can provide estimates of shallow convective mixing over broad regions. Note that the role of shallow convective mixing may be different in deep cumulus, shallow cumulus, and stratocumulus regions. In this paper, we focus on shallow cumulus regions because (1) shallow cumulus is the most frequent cloud type on Earth, and (2) its sensitivity to climate change greatly influences future climate projections (Bony et al., 2017).

Multiple studies have successfully demonstrated the utility of applying water isotope ratios to investigate the export of boundary layer moisture into the free troposphere (Bailey et al., 2013; Berkelhammer et al., 2012;

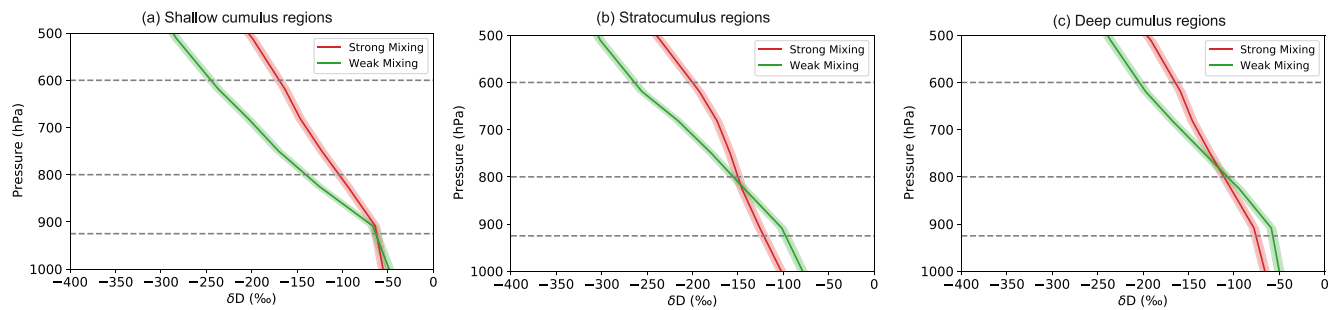


**Figure 2.** Profiles of water vapor  $\delta D$  retrieved from AIRS (2002–2019) in “strong”/“weak” mixing months over (a) shallow cumulus, (b) stratocumulus, and (c) deep cumulus regions between 30°S and 30°N. The dashed lines refer to 600, 800, and 925 hPa. The error bars represent two standard deviations of uncertainties in measured  $\delta D$  values.

Galewsky, 2018; Lee et al., 2011). The estimated convective mixing (i.e.,  $\delta D$ -diagnosed convective mixing) changes are analyzed alongside low-cloud properties from satellite retrievals to explore the influence of shallow convective mixing on low clouds.

Section 2 describes our data and methodology; Section 3 gives an overview of our results, and the implications of our findings are discussed in Section 4.

## 2. Data and Methods

### 2.1. Data

Estimates of water vapor  $\delta D$  are retrieved from NASA’s Atmospheric Infrared Sounder (AIRS) Lite version 6 data (Worden et al., 2019; 2002–2019). A sensitivity test for the consistency of our results is also performed with equivalent retrievals from NASA’s Tropospheric Emission Spectrometer (TES; Text S1 in Supporting Information S1). Only those retrievals with at least 0.5 degrees of freedom in HDO are selected to ensure the quality of the data (Bailey et al., 2017). The degrees of freedom (DOF) are defined as the fractional number of significant eigenfunctions used in the retrieval process, representing the fraction of the retrieved value derived directly from the satellite observations rather than prior estimates. Larger DOF indicate the retrievals are more representative of satellite measurements (Payne et al., 2009). A threshold of 0.5 DOF is sufficient for calculating the atmospheric gradient in water isotopes because the isotopic composition in the marine boundary layer is reasonably well constrained by exchange with the ocean, and the ocean itself varies in isotopic composition by only a few ‰. As a result, the vertical gradient will be largely determined by the midtropospheric isotopic composition, and, it is within this level that TES and AIRS are most sensitive. In addition, since the retrieval is sensitive to increased cloudiness, only those retrievals with an average cloud optical depth (COD) less than 3.6 are used.

Cloud properties, including cloud fractions and cloud heights, are derived from NASA’s Moderate Resolution Imaging Spectroradiometer (MODIS) Atmosphere Products MOD08 (Hubanks et al., 2016). In this study, low-level clouds are clouds with top pressures larger than 680 hPa, and high-level clouds are clouds with top pressures of less than 440 hPa (Rossow & Schiffer, 1991). As high clouds sometimes obscure or influence changes in low clouds, we employed the method described in Scott et al. (2020) to obtain the nonobscured low-cloud fraction. Atmospheric environmental variables such as air temperature, boundary layer top pressure, and relative humidity are extracted from AIRS retrievals. All satellite retrievals are binned and monthly averages are computed over  $5^\circ \times 5^\circ$  grid boxes, which have measurement uncertainty no larger than 8–10‰. Finally, we use the ERA5 reanalysis (Hersbach et al., 2020) to compare the  $\delta D$ -diagnosed convective mixing estimated in this study to the estimates defined by Sherwood et al. (2014).

### 2.2. Methods

As mentioned above, there is a sharp vertical gradient of water vapor  $\delta D$  between the boundary layer and the free troposphere (Figure 2). Shallow convective mixing exchanges air between these two layers and dampens (or reduces) the gradient of water vapor  $\delta D$ , such that areas with stronger convective mixing will exhibit smaller gradients in water vapor  $\delta D$  (Berkelhammer et al., 2012; Noone et al., 2011). Therefore, we use the gradient

of water vapor  $\delta D$  to represent (qualitatively) the amount of shallow convective mixing in a given region. We calculate the difference of water vapor  $\delta D$  between the free troposphere (600–800 hPa) and the boundary layer (800–925 hPa) to estimate shallow convective mixing. Our metric for estimating shallow convective mixing is as follows:

$$\Delta\delta D = \delta D_{\text{Layer 1}} - \delta D_{\text{Layer 2}} \quad (1)$$

where  $\Delta\delta D$  is the vertical isotopic gradient,  $\delta D_{\text{Layer 1}}$  is the layer-average  $\delta D$  representing the lower free troposphere, and  $\delta D_{\text{Layer 2}}$  is the layer-average  $\delta D$  representing the boundary layer. Layer 1 is defined as 600–800 hPa and Layer 2 as 800–925 hPa. We calculate the arithmetic mean of water vapor  $\delta D$  in both layers (Noone, 2012). We note that calculating the linear slopes of water vapor  $\delta D$  between 600 and 925 hPa by regressing  $\delta D$  on height is another way to estimate the vertical gradient of water vapor  $\delta D$ , and the result of this estimate is similar to the vertical difference of water vapor  $\delta D$  between the free troposphere and the boundary layer (Text S3 in Supporting Information S1). For simplicity, in this study we use the method of the layer-mean differences of water vapor  $\delta D$ .

In addition, Sherwood et al. (2014) proposed an  $S$  index metric, the difference of temperature and relative humidity between 700 and 850 hPa using reanalysis data, to represent distributions of shallow convective mixing in the deep convective regions of the tropics. We use  $S$ , computed from ERA5 (Hersbach et al., 2020), as an independent validation check on estimates of shallow convective mixing.

To distinguish shallow cumulus regimes from deep cumulus and stratocumulus regimes, we used the Cumulus And Stratocumulus CloudSat-CALIPSO Data set (CASCCAD; Cesana et al., 2019). The regions of deep cumulus, stratocumulus, and shallow cumulus include all grid cells where the climatological fraction of the corresponding cloud type is larger than 0.1, 0.3, and 0.2, respectively.

In order to investigate the impact of  $\delta D$ -diagnosed shallow convective mixing on low-cloud properties, composite analysis is employed. Months of strong and weak mixing are selected for each  $5^\circ \times 5^\circ$  grid box. “Strong”/“weak” months are selected when the monthly  $\delta D$ -diagnosed convective mixing exceeds one standard deviation ( $\pm 1\sigma$ ) of the convective mixing monthly mean of each grid box.

Finally, to rule out the influence of horizontal advection on the vertical  $\delta D$  gradient, we investigate horizontal advection of  $\delta D$ . The horizontal advection of water vapor  $\delta D$  is calculated as the gradient of water vapor isotope ratio multiplied by horizontal motion:  $-u\frac{\partial R}{\partial x} - v\frac{\partial R}{\partial y}$ , where  $R$  is the water isotope ratio (HDO/H<sub>2</sub>O),  $u$  is zonal wind, and  $v$  is meridional wind.

### 3. Results

#### 3.1. Estimates of Shallow Convective Mixing

##### 3.1.1. Estimates From Satellite Data

Climatological averages of seasonal  $\delta D$ -diagnosed shallow convective mixing, estimated by the vertical gradient of water vapor  $\delta D$  retrieved from AIRS, are shown in Figure 3. The general pattern of  $\delta D$ -diagnosed shallow convective mixing is similar to climatological rainfall.  $\delta D$ -diagnosed convective mixing is strong over the Warm Pool, the tropical Indian Ocean, and the equatorial Pacific and Atlantic; conversely, mixing is weak over the midlatitude gyres in the Pacific and the Atlantic. Seasonal variation of  $\delta D$ -diagnosed convective mixing follows the movement of the Intertropical Convergence Zone (ITCZ). To ensure our estimate of the gradient of water vapor  $\delta D$  from the AIRS data is meaningful, we calculate the error of the gradient of water vapor  $\delta D$  (Figure S1 in the Supporting Information S1). The error ranges from 8‰ to 10‰ in the tropics, which is much smaller than the differences shown in Figure 3. This indicates that the signal of the vertical difference of water vapor  $\delta D$  is strong, and not masked by the uncertainties of satellite retrievals. For completeness, we repeated this composite analysis using NASA’s Tropospheric Emission Spectrometer (TES; Text S1 and Figure S2 in the Supporting Information S1), because TES is more sensitive to variations of water vapor  $\delta D$  in the boundary layer and the vertical gradient of  $\delta D$ . We find that the results of TES and AIRS are qualitatively similar. Note that similar spatial patterns are also observed when estimating the vertical gradient of  $\delta D$  as the slope of the water vapor  $\delta D$  profile (Text S2 and Figure S3 in the Supporting Information S1).

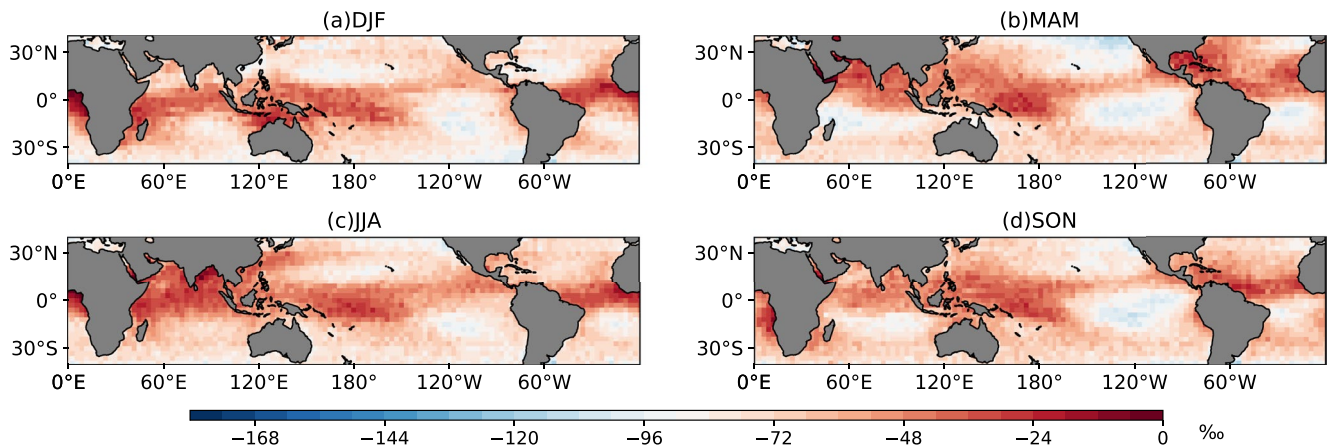


**Figure 3.** Climatological  $\delta D$ -diagnosed shallow convective mixing during four seasons estimated by the difference of the water vapor  $\delta D$  between the free troposphere (800–600 hPa) and the boundary layer (925–800 hPa) retrieved from AIRS (2002–2019).

### 3.1.2. Validating the Method of Isotopic Vertical Gradients

As a complement to the isotopic gradient analysis, we evaluated a similar metric for shallow convective mixing for comparison, the  $S$  index developed by (Sherwood et al., 2014), in Figure 4. The index is defined as the difference of relative humidity and temperature between 700 and 850 hPa:

$$S \equiv (\Delta H_{700-850}/100\% - \Delta T_{700-850}/9K) / 2 \quad (2)$$

where  $H$  is relative humidity and  $T$  is temperature (Figure 4). The spatial pattern of  $S$  is similar to the pattern resolved using  $\delta D$ -diagnosed convective mixing: strong mixing occurs over the Warm Pool and equatorial oceans, while weak mixing is observed around the center of the oceanic gyres. Similarly, the seasonal variation of the  $S$  index follows the movement of the ITCZ. As mentioned above, however, note that while the  $S$  index is an attempt to estimate shallow convective mixing, the gradient of relative humidity and temperature can also be controlled by radiation.

In order to further validate the  $\delta D$ -diagnosed shallow convective mixing, we analyzed the updraft detrainment rates averaged between 600 and 800 hPa from ERA5 (Hersbach et al., 2020). The detrainment rate indicates the rate at which a cloud moistens the ambient environment at a given vertical level. During shallow convective

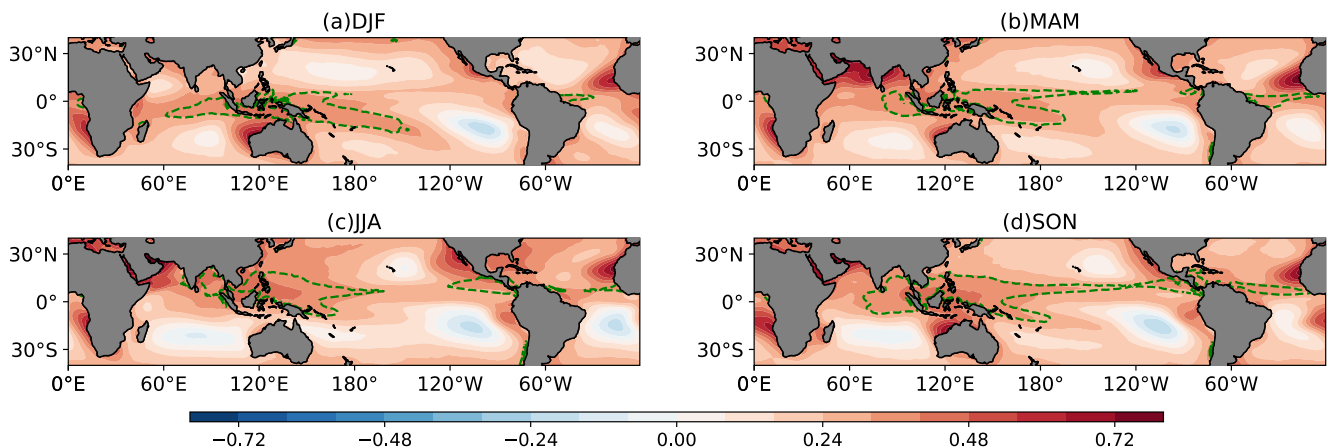


**Figure 4.** Climatological shallow convective mixing during boreal (a) winter, (b) spring, (c) summer, and (d) autumn estimated by the difference of relative humidity and temperature between 700 and 850 hPa (Sherwood et al., 2014) based on ERA5 (1979–2018). The green contours are the upper quartile of the annual-mean ascent rate at 500 hPa in ascending regions. The  $S$  index in the region enclosed by the green contours is averaged to get the global estimate of  $S$  values in Sherwood et al. (2014).

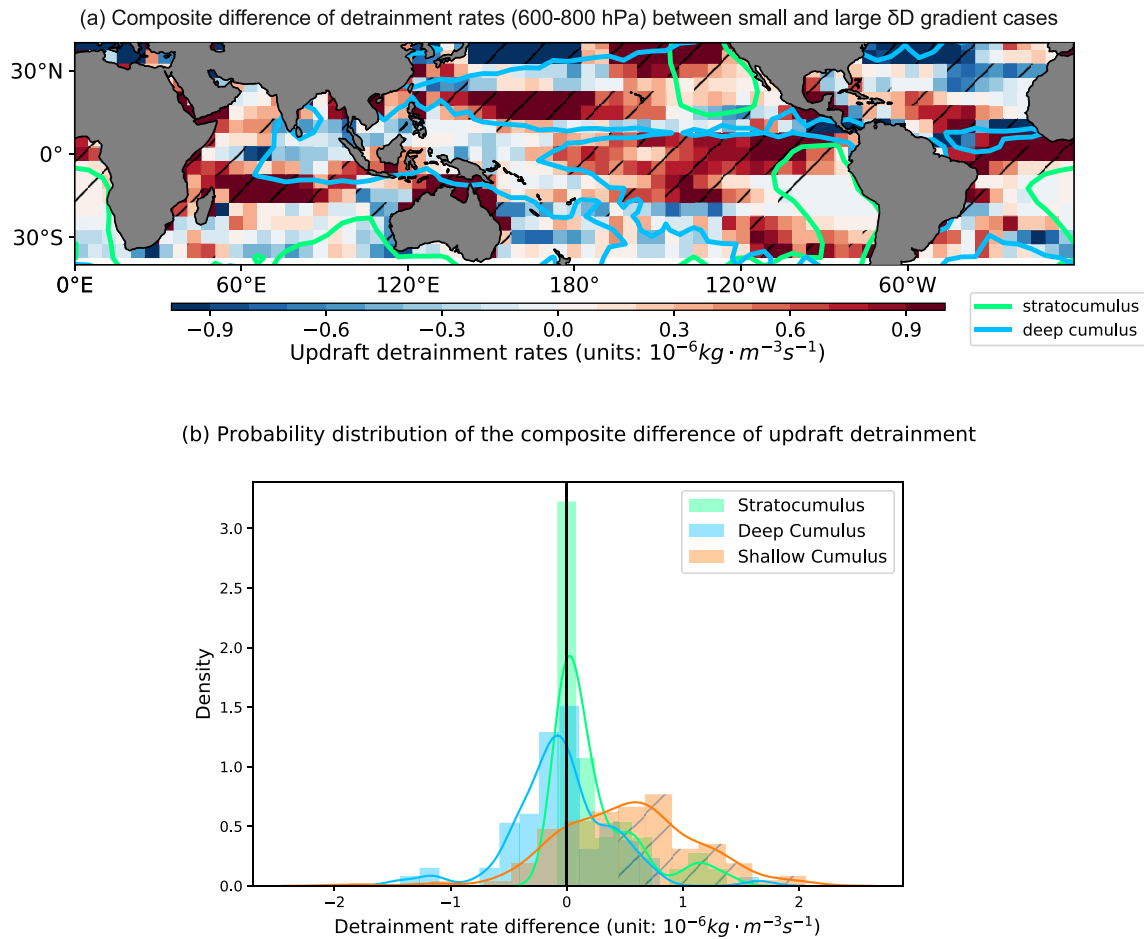


**Figure 5.** (a) Composite difference of the averaged updraft detrainment rates in 600–800 hPa between months with small and large vertical gradients of water vapor  $\delta D$  (see Section 2 for the selection thresholds). Hatched areas indicate the composite difference passes a two-sample  $t$  test at the 95% confidence level. The cyan and green thick lines enclose regions dominated by deep cumulus and stratocumulus, respectively. (b) The probability distribution of the composite difference values of each grid cell in (a) for deep cumulus (cyan), stratocumulus (green), and shallow cumulus (orange) regions. Hatched portions indicate the composite difference passes a two-sample  $t$  test at the 95% confidence level.

mixing, updrafts export moisture from the boundary layer into the free troposphere; moisture is detrained at the top-most levels of shallow convection. Thus, the updraft detrainment rate provides an estimate of the vertical transport of moisture due to shallow convection, which should represent shallow convective mixing. While we acknowledge that there may be (unquantified) biases in ERA5 detrainment (e.g., a slight overestimation of midtropospheric moisture in convective regions related to stronger shallow convection and detrainment than observed, Taszarek et al., 2021), we are nevertheless confident that the sign and significance of covariations between detrainment and  $\delta D$  vertical gradient should be an adequate test of the latter's ability to serve as a proxy for shallow convective mixing.

To examine the relationship between updraft detrainment and the vertical gradients of water vapor  $\delta D$ , we plotted the composite differences of updraft detrainment rate (averaged between 600 and 800 hPa) between months with small and large vertical gradients of water vapor  $\delta D$  (Figure 5). We also outline the regions of different cumulus types based on the CASCAD product (see Section 2 for details) to bolster the analysis: regions dominated by deep cumulus and stratocumulus are enclosed in cyan and green thick lines, respectively (Figure 5a). The remaining areas of the tropics are categorized as shallow cumulus regions. The result shows that in shallow cumulus regions, there is a strong positive relationship between updraft detrainment and vertical gradients of water vapor  $\delta D$ , and that this relationship is statistically significant. However, the relationship between updraft detrainment and vertical gradients of water vapor  $\delta D$  is not clear in deep cumulus and stratocumulus regions. To

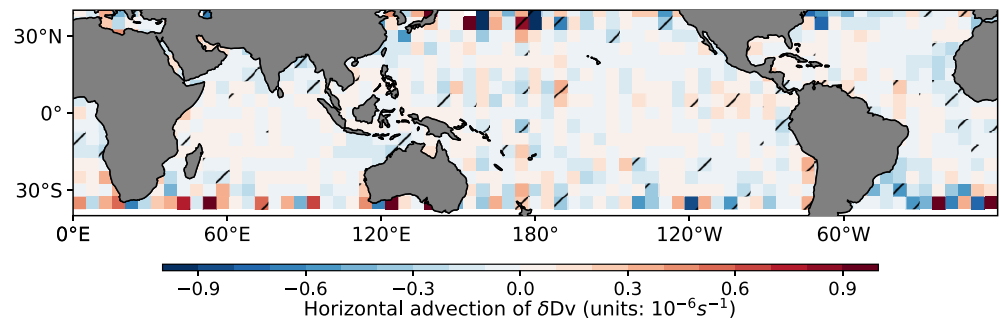


**Figure 6.** Composite difference of the horizontal advection of water vapor  $\delta D$  at 600 hPa (unit:  $10^{-6} \text{ s}^{-1}$ ) between strong and weak shallow convective mixing months. Hatched areas indicate the composite difference passes a two-sample  $t$  test at the 95% confidence level.

better summarize the results in these three cloud regions, Figure 5b shows the probability distribution of updraft detrainment differences between months of strong and weak  $\delta D$ -diagnosed shallow convective mixing as shown geographically in Figure 5a. Only in the shallow cumulus region does the relationship between updraft detrainment and water vapor  $\delta D$  gradients show a positive and statistically significant relationship, and grid boxes with statistically significant relationships comprise a large fraction (53%) of the region. For deep cumulus and stratocumulus regions, only 11% and 12% of the grid boxes, respectively, have a statistically significant relationship between updraft detrainment and water vapor  $\delta D$  gradients. If we take the measurement uncertainties of water vapor  $\delta D$  (about 8‰ in the tropics) into account, the result is still similar: 51% of the shallow cumulus region yields a positive and statistically significant relationship between updraft detrainment and water vapor  $\delta D$  gradients (Figure S5 in the Supporting Information S1). In summary, the steepness of the vertical gradient in water vapor  $\delta D$  accurately represents updraft detrainment, a proxy for shallow convective mixing in shallow cumulus regions in the tropics, but does not hold in deep cumulus or stratocumulus regions. Thus, we focus our subsequent analysis of shallow convective mixing's impacts (Section 3.2) on shallow cumulus regions.

In addition, horizontal advection can influence water vapor isotope ratios. To estimate the relative importance of horizontal mixing compared to vertical mixing, we analyzed a composite difference of horizontal advection of water vapor  $\delta D$  at 600 hPa between strong and weak convective months (Figure 6). The result shows that there are very few grid boxes with statistically significant relationships between  $\delta D$ -diagnosed shallow convective mixing and horizontal advection. This reassures us that horizontal advection does not obfuscate the shallow convective mixing signal in the regions pertinent to this study.

Like horizontal advection, large-scale vertical motions can also influence free tropospheric water vapor isotope ratios. Specifically, strong subsidence in shallow cumulus regions may cause free tropospheric  $\delta D$  to become more negative, leading to a larger gradient between the boundary layer and the free troposphere. Strong subsidence can also influence the strength of shallow convective mixing. In order to investigate the joint influence of subsidence and convective mixing on the  $\delta D$  gradients at monthly scales, we conducted a multivariate linear regression with two regressors: subsidence rates (averaged between 600 and 800 hPa) and detrainment rates (averaged between 600 and 800 hPa). The seasonal cycles of all three variables are removed, and all variables are standardized prior to regression. Therefore, the values of the regression coefficients for subsidence rates and detrainment rates can be directly compared to determine which factor is more important for the variation of  $\delta D$  gradients. Figure S6 in the Supporting Information S1 (where the sign for the subsidence field is flipped to enable direct comparison with the contribution from detrainment rates) shows that subsidence does have a significant influence on  $\delta D$  gradients, but the regression coefficients for the detrainment rates are much larger than the coefficients for subsidence rates in shallow cumulus regions. This indicates that the variations in the isotopic lapse rate are more sensitive to variations in convective mixing from below than to subsidence in shallow cumulus regions.

To better account for the possibility that interactions between subsidence and shallow convective detrainment inflate correlations between the  $\delta D$  gradient and detrainment, we also evaluated the partial correlations between these variables. Partial correlations measure the correlation between two variables while accounting for the

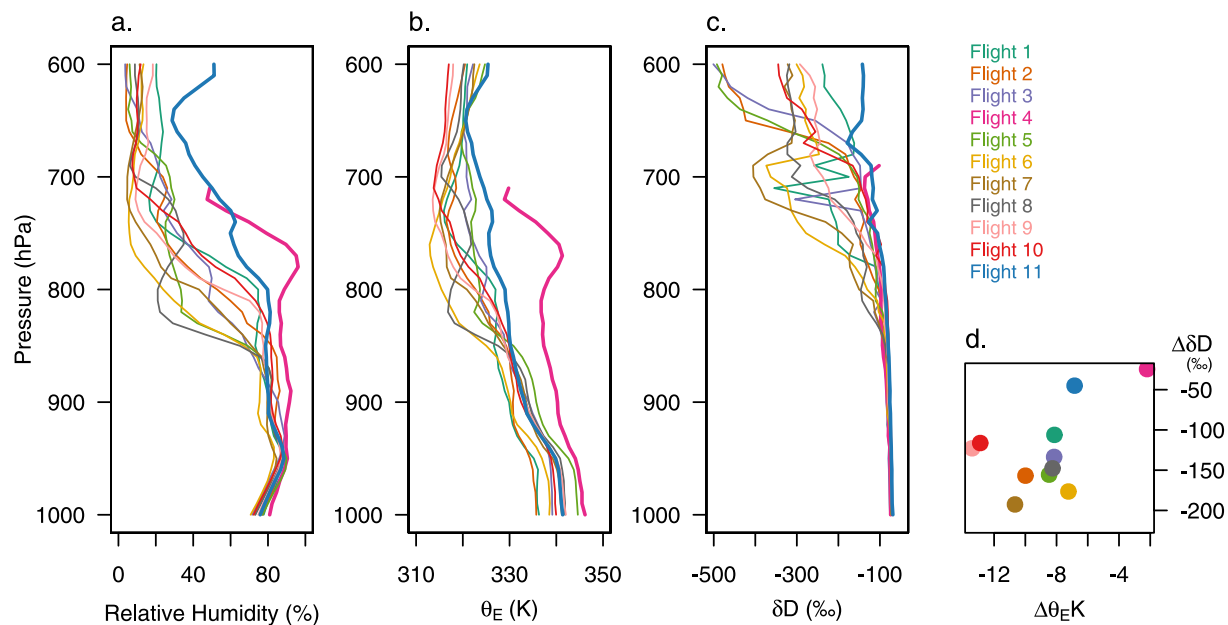


**Figure 7.** Flight-average vertical profiles of relative humidity (a), equivalent potential temperature (b), and water vapor  $\delta D$  (c) near Barbados from January 17 to February 11, 2020 observed by aircraft during the EUREC<sup>4</sup>A field campaign. The thicker pink and blue profiles (representing Flights 4 and 11, respectively) feature smaller vertical gradients of relative humidity, equivalent potential temperature, and water vapor  $\delta D$ , indicating 2 days of strong convective mixing. (d) Scatterplot of the vertical gradient of water vapor  $\delta D$  and  $\theta_E$  from 11 flights.

possible confounding influence of a third. Figure S7 in the Supporting Information S1 shows that the  $\delta D$ -gradient is much more strongly correlated with detrainment (when controlling for subsidence) than with subsidence (when controlling for detrainment), indicating that  $\delta D$  in the lower free troposphere responds more sensitively to mixing from below than to sinking air motions from above. This is not to say that subsidence does not affect the  $\delta D$ -gradient; only that, for a given subsidence rate, there are significant covariations in the  $\delta D$ -gradient and shallow convective detrainment driven by mixing from below.

As an additional check on how well the  $\delta D$  vertical gradient represents shallow convective mixing, gradients were calculated from the water isotopic data collected by the NOAA P-3 aircraft during the 2020 EUREC<sup>4</sup>A field campaign. One of the primary science goals of EUREC<sup>4</sup>A was to evaluate shallow convective mixing in the western tropical Atlantic, near the island of Barbados (Bailey et al., 2022; Stevens et al., 2021). Figure 7 shows mean profiles (with 10-hPa vertical spacing) of relative humidity, equivalent potential temperature, and  $\delta D$  for the 11 P-3 flights (Pincus et al., 2021). As evidenced by Figure 7, both Flights 4 and 11 are more humid aloft and are characterized by higher moist static energy (i.e., higher  $\theta_E$ ) in the 700–850 hPa layer, consistent with stronger shallow convective mixing. As expected, the  $\delta D$  profiles for both flights are characterized by a weaker gradient in the vertical. Vertical gradients of  $\theta_E$  and water vapor  $\delta D$  in other flights are also closely related, as shown in Figure 7d. (The relative humidity and equivalent potential temperature were measured by dropsondes released from the plane, while  $\delta D$  was measured using an on-board isotopic analyzer. Thus, the pool of data available from the dropsondes exceeds that of the water isotope data, and the profiles from the former are smoother.)

The Supporting Information S1 contains two final sensitivity tests (Texts S4 and S5 in Supporting Information S1). Table S1 in the Supporting Information S1 includes estimates of the  $\delta D$  gradients from the 11 P-3 flights calculated using the same two-layer difference as applied to the satellite retrievals (Equation 1) but with different layer depths and/or different averaging techniques. Flights 4 and 11 consistently stand out for their relatively weak gradients, indicating that our ability to detect shallow convective mixing is fairly insensitive to the exact method by which the two  $\delta D$  layers are defined. Additionally, apart from vertical mixing and horizontal advection, Rayleigh distillation in condensation processes also influences water vapor isotopic values. In Text S5 in the Supporting Information S1, we discuss the effect of Rayleigh distillation by using a  $\ln q - \delta D$  framework. The result confirms that our estimation of shallow convective mixing by vertical isotopic gradients is reliable when considering the effect of Rayleigh distillation.



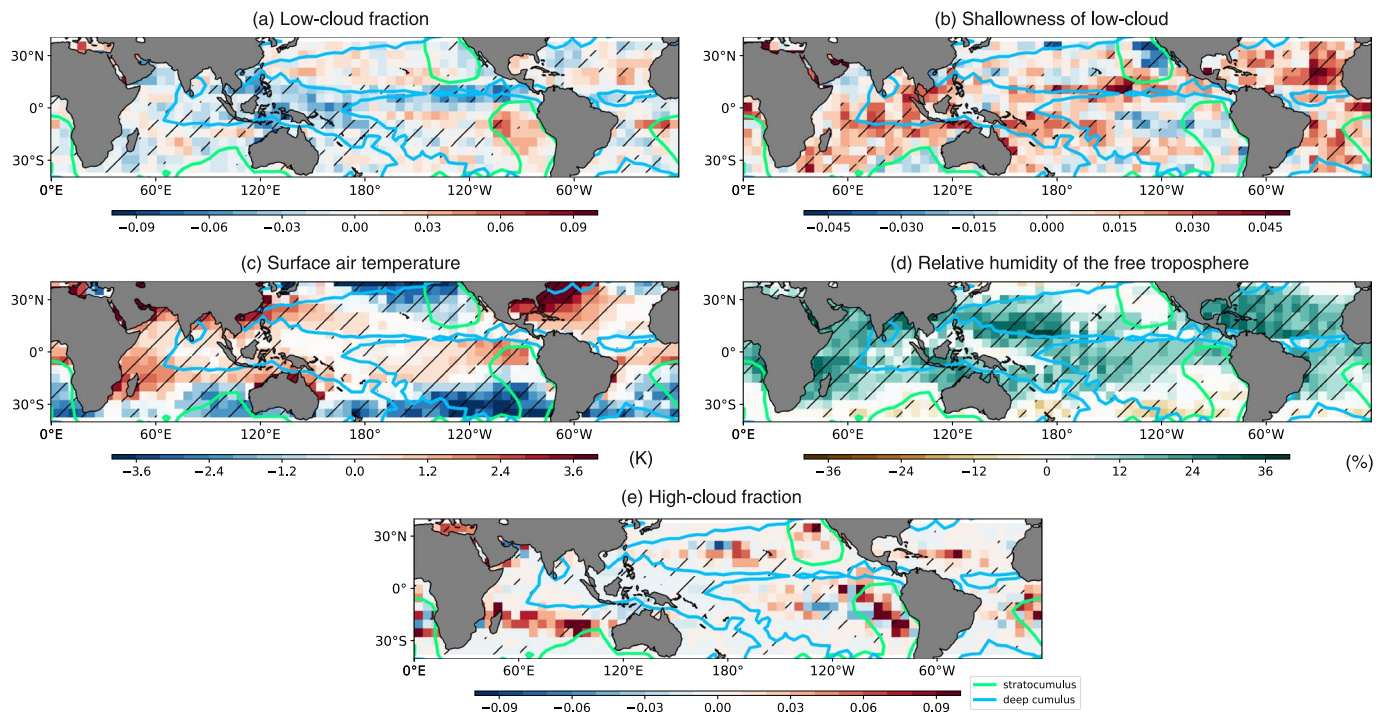


**Figure 8.** Composite difference of (a) low-cloud fraction (unitless, Moderate Resolution Imaging Spectroradiometer (MODIS) data), (b) the shallowness of low clouds defined in Equation 4, (c) surface air temperature (K, Atmospheric Infrared Sounder (AIRS) data), (d) relative humidity of the free troposphere (averaged between 600 and 800 hPa, unit: %, AIRS data), and (e) high-cloud fraction (unitless, MODIS data) between strong and weak shallow convective mixing months. Hatched areas indicate the composite difference passes a two-sample *t* test at the 95% confidence level. The cyan and green thick lines enclose regions dominated by deep cumulus and stratocumulus, respectively.

### 3.2. Impact of Shallow Convective Mixing on Low-Cloud Properties

The composite differences of low-cloud properties for strong versus weak shallow convective months are shown in Figure 8. Since our  $\delta D$ -diagnosed shallow convective mixing works best in the shallow cumulus regions, we focus on these regions. In the shallow cumulus regions (the southern Indian Ocean and gyre regions of the Pacific and Atlantic), the relationships between  $\delta D$ -diagnosed convective mixing and nonobscured low-cloud fraction are generally weak and heterogeneous, and not statistically significant (Figure 8a). For example, strong convective mixing is associated with reduced low-cloud fraction over the South Pacific gyre, but corresponds to a higher low-cloud fraction in the northeastern Atlantic. We note that reduced low-cloud fraction is associated with increased convective mixing in the deep cumulus regions, but the result is questionable because our estimations of convective mixing may be not accurate enough in those regions, as shown in Figure 5. Although the relationship between  $\delta D$ -diagnosed shallow convective mixing and low-cloud fraction is variable in the shallow cumulus regions, the associations between shallow convective mixing and other environmental factors exhibit patterns in line with we expect: strong shallow convective mixing moistens the free troposphere (Figure 8d) and strong convective mixing is associated with warmer surface temperature (Figure 8c). The moistening of the free troposphere with strong convective mixing is consistent with Sherwood et al. (2014): convective mixing moistens the free troposphere at the expense of the boundary layer.

To consider the influence of subsidence on the relationship between mixing and cloud cover, we calculated the partial correlations between the  $\delta D$ -gradient and low-cloud fraction, after controlling for the effects of subsidence (Figure S8 in the Supporting Information S1). The result is similar to Figure 8a: the low-cloud response to increased shallow convective mixing is variable and frequently insignificant in shallow cumulus regions. Thus, the spatially-variable relationship between convective mixing and low-cloud fraction still holds when we control for the effects of subsidence. (Interestingly, the relationship between the  $\delta D$ -diagnosed convective mixing and low-cloud fraction is no longer dominantly negative in the Warm Pool region, which may indicate that the negative relationship over the Warm Pool shown in Figure 8a is largely driven by subsidence—another reason why we recommend applying the isotopic metric to shallow cumulus regions only.)

To characterize other changes in the low-cloud fraction due to  $\delta D$ -diagnosed shallow convective mixing, we analyzed the vertical distribution of low-cloud fraction. Previous studies (Brient et al., 2016; Nuijens et al., 2015a, 2015b) have shown that the variations of low clouds at the lifting condensation level (LCL) and clouds aloft near the trade wind inversion are remarkably different. Brient et al. (2016) define a new metric, a “shallowness index” to describe the vertical distributions of low-levels clouds. Their shallowness index  $\gamma$  is defined by:

$$\gamma = \frac{CF_{950}}{(CF_{850} + CF_{950})}, \quad (3)$$

where  $CF_{950}$  and  $CF_{850}$  are the low-cloud fractions at 950 and 850 hPa. Here we employ a revised version of this index  $\gamma'$  to explore the responses of vertical distributions of low-levels clouds to shallow convective mixing (Figure 8b). Our change to the metric is due to the fact that MODIS only provides cloud fraction of clouds with top pressures within a given range (instead of cloud fraction at a given level). The revised shallowness index  $\gamma'$  is defined by:

$$\gamma' = \frac{CF_{>920}}{(CF_{800-920} + CF_{>920})}, \quad (4)$$

where  $CF_{>920}$  and  $CF_{800-920}$  are the low-cloud fractions with cloud tops  $>920$  hPa and between 800 and 920 hPa, respectively. Figure 8b shows that the low clouds are shallower with increased shallow convective mixing over a large fraction of the Indian Ocean and tropical Atlantic. This is consistent with LES results that suggest low clouds are shallower when convective mixing is stronger (Vial et al., 2017). Furthermore, Figure 8e shows that the high-cloud fraction varies little with shallow convective mixing over the tropics. This result demonstrates that the changes in low clouds are associated with the variations in shallow convective mixing, not with variations in deep convection.

In summary, our results suggest that in the shallow cumulus regions, the relationship between shallow convective mixing and low-cloud fraction is weak and not uniform, but that strong shallow convective mixing is associated with a moistening of the lower free troposphere.

#### 4. Discussion and Conclusions

Low-cloud feedbacks are not fully understood in observations or climate models, generating substantial uncertainties in future climate projections (Sherwood et al., 2014; Zelinka et al., 2020). In particular, the role of shallow convective mixing on low-cloud processes is under-constrained (Blossey et al., 2013; Brient et al., 2016; Vial et al., 2016, 2017). However, there are few observational estimates of shallow convective mixing. In this study, we address this and demonstrate that the vertical gradients of water vapor stable isotopes from satellite retrievals can be used to estimate shallow convective mixing. Our estimations are comparable with the updraft detrainment rates from ERA5 reanalysis data and other indices of shallow convective mixing (Sherwood et al., 2014), but our estimation using water vapor isotopes is not sensitive to shortwave and longwave radiation in the way other metrics, which involve temperature and relative humidity, are. As compared to the work of Sherwood et al. (2014), which suggests a link between shallow convective mixing in deep convective regions and low clouds in shallow cumulus regions, our work focuses on the direct connection between convective mixing and low clouds in shallow cumulus regions. We find that there are no strong relationships between shallow convective mixing and low-cloud fraction in the shallow cumulus regions. The satellite-derived observations suggest the relationship between shallow convective mixing and low-cloud fraction is heterogeneous.

There are uncertainties and shortcomings in our isotopic proxy for shallow convective mixing that are important to acknowledge. First, there are noticeable uncertainties in the satellite retrievals of water vapor stable isotopes. Satellites do not directly measure stable isotopes, but retrieve the column-integrated radiance influenced by water isotopes. The water vapor stable isotopes are calculated by retrieval algorithms that involve averaging kernels (Worden et al., 2006, 2019), and several key uncertainties exist in these algorithms. Inherently wide averaging kernels also limit the vertical resolution of the satellite retrievals, while shallow convective mixing occurs over a limited vertical range. Second, it takes about 2 weeks for satellites (e.g., AIRS) to finish a full observation over the globe, so our estimations are limited to monthly and seasonal timescales. Although these timescales are relevant

to scientific questions surrounding the influence of climate change on low clouds, data monthly or seasonal timescales hinders examination of fast-timescale processes affecting low clouds, such as the temporary shoaling of low clouds in the “cumulus valve mechanism” (Vial et al., 2017). Moreover, although vertical mixing is the dominant process influencing the isotopic gradients in the subsidence-dominated regions (Bailey et al., 2015; Blossy et al., 2010), several processes including evaporation, condensation, and precipitation govern the water isotopic content of the lower troposphere (Risi et al., 2020). While we have considered the influence of Rayleigh distillation in the Supporting Information S1, further deconvolution of the isotopic effects of vertical mixing from other processes (e.g., evaporation and condensation/precipitation processes) would enhance this analysis.

Precipitation is also an important factor influencing low-cloud formation. As convection develops, precipitation limits cloud layer deepening and free tropospheric moistening by reducing the liquid water available for evaporation (Vogel et al., 2016). Reevaporation of falling raindrops can also humidify the subcloud layer, enhancing the moisture available for new cloud development. In contrast, precipitation in organized convection may be associated with reduced cloud coverage (Seifert & Heus, 2013). In future work, we intend to evaluate how precipitation regulates the response of low cloud to  $\delta D$ -diagnosed shallow convective mixing.

Despite these potential limitations, a key advantage to using satellite retrievals of water vapor isotopes is that they permit estimation of shallow convective mixing across a broad geographic area, facilitating the evaluation of GCMs in the responses of their low-cloud fraction to shallow convective mixing. While many climate models simulate reduced low-cloud fraction with strong shallow convective mixing, LES suggest that GCMs may erroneously amplify this positive feedback. Indeed, most LES suggest that cloud fraction is largely insensitive to variations in the strength of shallow convective mixing (Vial et al., 2017), and our study seems to provide evidence that backs this assertion. Our estimation of changes in low-cloud properties as a result of convective mixing can be used as a reference (i.e., an extra degree of freedom) to evaluate the simulation of low clouds in GCMs, guiding model development and refinement of parameters in convection, cloud, and boundary layer schemes to better simulate low-cloud processes. Specifically, bias of the  $\delta D$  gradient-low clouds relationship in isotope-enabled models may help diagnose deficiencies in shallow and deep convection schemes.

In forthcoming work, we envision sensitivity tests to identify which convection and cloud-related model parameters most significantly influence the relationships between low-cloud and the  $\delta D$ -diagnosed shallow convective mixing. Climate sensitivity estimates may be refined by tuning model parameters (e.g., entrainment rates and reevaporation rates) to match the cloud-mixing relationship highlighted in this work. In addition, if convective mixing simulated by models in the modern period is positively correlated to the climate sensitivity of those models, this empirical relationship may be considered an *emergent constraint* improving model climate sensitivity (Klein & Hall, 2015). In future work, we hope to identify whether or not the  $\delta D$ -diagnosed shallow convective mixing provides useful, complementary *emergent constraints* on climate model physics and sensitivity.

In conclusion, this study provides a novel approach for estimating shallow convective mixing using stable water isotopes from remote sensing products. Given the increased values and large uncertainties of estimated climate sensitivity simulated by the latest state-of-the-art model versions (Meehl et al., 2020; Zelinka et al., 2020), this work provides a framework and first step toward better constraints on factors influencing low-cloud properties, informing projections of future anthropogenic warming.

### Conflict of Interest

The authors declare no conflicts of interest relevant to this study.

### Data Availability Statement

Data products from NASA's AIRS, TES, and MODIS can be downloaded from <https://search.earthdata.nasa.gov/search>. ERA5 data can be downloaded from the Climate Data Store (<https://cds.climate.copernicus.eu/#/home>). The CASCCAD data can be accessed from <https://data.giss.nasa.gov/clouds/casccad/>. EUREC<sup>4</sup>A data can be downloaded from <https://doi.org/10.25921/c5yx-7w29> (isotope data) and <https://doi.org/10.25326/246> (dropsondes data, including relative humidity and  $\theta_p$ ).

## Acknowledgments

We thank two anonymous reviewers for their constructive comments. This work was funded by NASA ROSES: Weather and Atmospheric Dynamics (NNH19ZDA001N-ATDM). This material is based upon work supported by the National Center for Atmospheric Research, which is a major facility sponsored by the National Science Foundation under Cooperative Agreement 1852977. Part of the research was carried out at the Jet Propulsion Laboratory, California Institute of Technology, under a contract with the National Aeronautics and Space Administration.

## References

- Bailey, A., Aemisegger, F., Villiger, L., Los, S. A., Reverdin, G., Quiñones Meléndez, E., & Thompson, E. (2022). Isotopic measurements in water vapor, precipitation, and seawater during EUREC<sup>4</sup>A. *Earth System Science Data Discussions*, 2022, 1–40. <https://doi.org/10.5194/essd-2022-3>
- Bailey, A., Blossey, P., Noone, D., Nusbaumer, J., & Wood, R. (2017). Detecting shifts in tropical moisture imbalances with satellite-derived isotope ratios in water vapor. *Journal of Geophysical Research: Atmospheres*, 122, 5763–5779. <https://doi.org/10.1002/2016JD026222>
- Bailey, A., Nusbaumer, J., & Noone, D. (2015). Precipitation efficiency derived from isotope ratios in water vapor distinguishes dynamical and microphysical influences on subtropical atmospheric constituents. *Journal of Geophysical Research: Atmospheres*, 120, 9119–9137. <https://doi.org/10.1002/2015JD023403>
- Bailey, A., Posmentier, E., & Feng, X. (2018). Patterns of evaporation and precipitation drive global isotopic changes in atmospheric moisture. *Geophysical Research Letters*, 45, 7093–7101. <https://doi.org/10.1029/2018GL078254>
- Bailey, A., Toohy, D., & Noone, D. (2013). Characterizing moisture exchange between the Hawaiian convective boundary layer and free troposphere using stable isotopes in water. *Journal of Geophysical Research: Atmospheres*, 118, 8208–8221. <https://doi.org/10.1002/jgrd.50639>
- Berkelhammer, M., Risi, C., Kurita, N., & Noone, D. C. (2012). The moisture source sequence for the Madden-Julian Oscillation as derived from satellite retrievals of HDO and H<sub>2</sub>O. *Journal of Geophysical Research*, 117, D03106. <https://doi.org/10.1029/2011JD016803>
- Blossey, P. N., Bretherton, C. S., Zhang, M., Cheng, A., Endo, S., Heus, T., & Xu, K.-M. (2013). Marine low cloud sensitivity to an idealized climate change: The CGILS LES intercomparison. *Journal of Advances in Modeling Earth Systems*, 5, 234–258. <https://doi.org/10.1002/jame.20025>
- Blossey, P. N., Kuang, Z., & Roms, D. M. (2010). Isotopic composition of water in the tropical tropopause layer in cloud-resolving simulations of an idealized tropical circulation. *Journal of Geophysical Research*, 115, D24309. <https://doi.org/10.1029/2010JD014554>
- Bony, S., Stevens, B., Ament, F., Bigorre, S., Chazette, P., Crewell, S., & Wirth, M. (2017). EUREC4A: A field campaign to elucidate the couplings between clouds, convection and circulation. *Surveys in Geophysics*, 38(6), 1529–1568. <https://doi.org/10.1007/s10712-017-9428-0>
- Boucher, O., Randall, D., Artaxo, P., Bretherton, C., Feingold, G., Forster, P., et al. (2013). Clouds and aerosols. In *Climate change 2013: The physical science basis. Contribution of working group I to the fifth assessment report of the intergovernmental panel on climate change* (pp. 571–657). Cambridge University Press.
- Brient, F., Schneider, T., Tan, Z., Bony, S., Qu, X., & Hall, A. (2016). Shallowness of tropical low clouds as a predictor of climate models' response to warming. *Climate Dynamics*, 47(1), 433–449. <https://doi.org/10.1007/s00382-015-2846-0>
- Cesana, G., Del Genio, A. D., & Chepfer, H. (2019). The cumulus and stratocumulus CloudSat-CALIPSO Dataset (CASCCAD). *Earth System Science Data*, 11(4), 1745–1764. <https://doi.org/10.5194/essd-11-1745-2019>
- Galewsky, J. (2018). Using stable isotopes in water vapor to diagnose relationships between lower-tropospheric stability, mixing, and low-cloud cover near the island of Hawaii. *Geophysical Research Letters*, 45, 297–305. <https://doi.org/10.1002/2017GL075770>
- Galewsky, J., Steen-Larsen, H. C., Field, R. D., Worden, J., Risi, C., & Schneider, M. (2016). Stable isotopes in atmospheric water vapor and applications to the hydrologic cycle. *Reviews of Geophysics*, 54, 809–865. <https://doi.org/10.1002/2015RG000512>
- Galewsky, J., Strong, M., & Sharp, Z. D. (2007). Measurements of water vapor D/H ratios from Mauna Kea, Hawaii, and implications for subtropical humidity dynamics. *Geophysical Research Letters*, 34, L22808. <https://doi.org/10.1029/2007GL031330>
- Hersbach, H., Bell, B., Berrisford, P., Hirahara, S., Horányi, A., Muñoz-Sabater, J., & Thépaut, J.-N. (2020). The ERA5 global reanalysis. *Quarterly Journal of the Royal Meteorological Society*, 146(730), 1999–2049. <https://doi.org/10.1002/qj.3803>
- Hubanks, P. A., King, M. D., Platnick, S., & Pincus, R. (2016). *Modis atmosphere l3 gridded product algorithm theoretical basis document ATBD* Ref. No. ATBD-MOD-30, 96.
- Klein, S. A., & Hall, A. (2015). Emergent constraints for cloud feedbacks. *Current Climate Change Reports*, 1(4), 276–287. <https://doi.org/10.1007/s40641-015-0027-1>
- Lee, J., Worden, J., Noone, D., Bowman, K., Eldering, A., LeGrande, A., & Sodemann, H. (2011). Relating tropical ocean clouds to moist processes using water vapor isotope measurements. *Atmospheric Chemistry and Physics*, 11(2), 741–752. <https://doi.org/10.5194/acp-11-741-2011>
- Meehl, G. A., Senior, C. A., Eyring, V., Flato, G., Lamarque, J.-F., Stouffer, R. J., & Schlund, M. (2020). Context for interpreting equilibrium climate sensitivity and transient climate response from the CMIP6 Earth system models. *Science Advances*, 6(26), eaba1981. <https://doi.org/10.1126/sciadv.aba1981>
- Noone, D. (2012). Pairing measurements of the water vapor isotope ratio with humidity to deduce atmospheric moistening and dehydration in the tropical midtroposphere. *Journal of Climate*, 25(13), 4476–4494. <https://doi.org/10.1175/JCLI-D-11-00582.1>
- Noone, D., Galewsky, J., Sharp, Z. D., Worden, J., Barnes, J., Baer, D., & Wright, J. S. (2011). Properties of air mass mixing and humidity in the subtropics from measurements of the D/H isotope ratio of water vapor at the Mauna Loa Observatory. *Journal of Geophysical Research*, 116, D22113. <https://doi.org/10.1029/2011JD015773>
- Nuijens, L., Medeiros, B., Sandu, I., & Ahlgrimm, M. (2015a). The behavior of trade-wind cloudiness in observations and models: The major cloud components and their variability. *Journal of Advances in Modeling Earth Systems*, 7, 600–616. <https://doi.org/10.1002/2014MS000390>
- Nuijens, L., Medeiros, B., Sandu, I., & Ahlgrimm, M. (2015b). Observed and modeled patterns of covariability between low-level cloudiness and the structure of the trade-wind layer. *Journal of Advances in Modeling Earth Systems*, 7, 1741–1764. <https://doi.org/10.1002/2015MS000483>
- Payne, V. H., Clough, S. A., Shephard, M. W., Nassar, R., & Logan, J. A. (2009). Information-centered representation of retrievals with limited degrees of freedom for signal: Application to methane from the Tropospheric Emission Spectrometer. *Journal of Geophysical Research*, 114, D10307. <https://doi.org/10.1029/2008JD010155>
- Pincus, R., Fairall, C. W., Bailey, A., Chen, H., Chuang, P. Y., de Boer, G., & Zuidema, P. (2021). Observations from the NOAA P-3 aircraft during ATOMIC. *Earth System Science Data Discussions*, 2021, 1–25. <https://doi.org/10.5194/essd-2021-11>
- Rauber, R. M., Stevens, B., Ochs, H. T., Knight, C., Albrecht, B. A., Blyth, A. M., & Zuidema, P. (2007). Rain in shallow cumulus over the ocean: The RICO campaign. *Bulletin of the American Meteorological Society*, 88(12), 1912–1928. <https://doi.org/10.1175/BAMS-88-12-1912>
- Rémillard, J., Kollias, P., Luke, E., & Wood, R. (2012). Marine boundary layer cloud observations in the Azores. *Journal of Climate*, 25(21), 7381–7398. <https://doi.org/10.1175/JCLI-D-11-00610.1>
- Risi, C., Muller, C., & Blossey, P. (2020). What controls the water vapor isotopic composition near the surface of tropical oceans? Results from an analytical model constrained by large-eddy simulations. *Journal of Advances in Modeling Earth Systems*, 12, e2020MS002106. <https://doi.org/10.1029/2020MS002106>
- Rossow, W. B., & Schiffer, R. A. (1991). ISCCP cloud data products. *Bulletin of the American Meteorological Society*, 72(1), 2–20. [https://doi.org/10.1175/1520-0477\(1991\)072<0002:ICDP>2.0.CO;2](https://doi.org/10.1175/1520-0477(1991)072<0002:ICDP>2.0.CO;2)
- Scott, R. C., Myers, T. A., Norris, J. R., Zelinka, M. D., Klein, S. A., Sun, M., & Doelling, D. R. (2020). Observed sensitivity of low-cloud radiative effects to meteorological perturbations over the global oceans. *Journal of Climate*, 33(18), 7717–7734. <https://doi.org/10.1175/JCLI-D-19-1028.1>

- Seifert, A., & Heus, T. (2013). Large-eddy simulation of organized precipitating trade wind cumulus clouds. *Atmospheric Chemistry and Physics*, 13(11), 5631–5645. <https://doi.org/10.5194/acp-13-5631-2013>
- Sherwood, S. C., Bony, S., & Dufresne, J.-L. (2014). Spread in model climate sensitivity traced to atmospheric convective mixing. *Nature*, 505(7481), 37–42. <https://doi.org/10.1038/nature12829>
- Siler, N., Bailey, A., Roe, G. H., Buizert, C., Markle, B., & Noone, D. (2021). The large-scale, long-term coupling of temperature, hydrology, and water isotopes. *Journal of Climate*, 34, 6725–6742. <https://doi.org/10.1175/JCLI-D-20-0563.1>
- Stevens, B., Bony, S., Farrell, D., Ament, F., Blyth, A., Fairall, C., & Zöger, M. (2021). EUREC<sup>4</sup>A. *Earth System Science Data*, 13(8), 4067–4119. <https://doi.org/10.5194/essd-13-4067-2021>
- Taszarek, M., Pilgaj, N., Allen, J. T., Gensini, V., Brooks, H. E., & Szuster, P. (2021). Comparison of convection parameters derived from ERA5 and MERRA-2 with rawinsonde data over Europe and North America. *Journal of Climate*, 34(8), 3211–3237. <https://doi.org/10.1175/JCLI-D-20-0484.1>
- Vial, J., Bony, S., Dufresne, J.-L., & Roehrig, R. (2016). Coupling between lower-tropospheric convective mixing and low-level clouds: Physical mechanisms and dependence on convection scheme. *Journal of Advances in Modeling Earth Systems*, 8, 1892–1911. <https://doi.org/10.1002/2016MS000740>
- Vial, J., Bony, S., Stevens, B., & Vogel, R. (2017). Mechanisms and model diversity of trade-wind shallow cumulus cloud feedbacks: A review. In *Shallow clouds, water vapor, circulation, and climate sensitivity* (pp. 159–181). Springer. [https://doi.org/10.1007/978-3-319-77273-8\\_8](https://doi.org/10.1007/978-3-319-77273-8_8)
- Vogel, R., Nuijens, L., & Stevens, B. (2016). The role of precipitation and spatial organization in the response of trade-wind clouds to warming. *Journal of Advances in Modeling Earth Systems*, 8, 843–862. <https://doi.org/10.1002/2015MS000568>
- Worden, J. R., Bowman, K., Noone, D., Beer, R., Clough, S., Eldering, A., & Worden, H. (2006). Tropospheric Emission Spectrometer observations of the tropospheric HDO/H<sub>2</sub>O ratio: Estimation approach and characterization. *Journal of Geophysical Research*, 111, D16309. <https://doi.org/10.1029/2005JD006606>
- Worden, J. R., Kulawik, S. S., Fu, D., Payne, V. H., Lipton, A. E., Polonsky, I., & Bowman, K. W. (2019). Characterization and evaluation of AIRS-based estimates of the deuterium content of water vapor. *Atmospheric Measurement Techniques*, 12(4), 2331–2339. <https://doi.org/10.5194/amt-12-2331-2019>
- Zelinka, M. D., Myers, T. A., McCoy, D. T., Po-Chedley, S., Caldwell, P. M., Ceppi, P., & Taylor, K. E. (2020). Causes of higher climate sensitivity in CMIP6 models. *Geophysical Research Letters*, 47, e2019GL085782. <https://doi.org/10.1029/2019GL085782>

## References From the Supporting Information

- Dee, S. G., Nusbaumer, J., Bailey, A., Russell, J. M., Lee, J.-E., Konecky, B., & Noone, D. C. (2018). Tracking the strength of the walker circulation with stable isotopes in water vapor. *Journal of Geophysical Research: Atmospheres*, 123, 7254–7270. <https://doi.org/10.1029/2017JD027915>
- Majoube, M. (1971). Fractionnement en oxygene 18 et en deuterium entre l'eau et sa vapeur. *Journal de Chimie Physique*, 68, 1423–1436. <https://doi.org/10.1051/jcp/1971681423>